A study on particle time-step and particle residence time discrepancies in 3D numerical hydrocyclone modeling

Orçun Ekin[*]

Aydın Adnan Menderes University, Faculty of Engineering, Mechanical Engineering Dept., Aytepe Mevkii, Efeler, PK: 09100, Aydın, Turkiye

Abstract. Short-circuit flow (SCF) or the flow of unseparated fluid skirting the separation process, frequently lowers the hydrocyclone effectiveness and overall efficiency. To address the problem of SCF, annular vortex finder hydrocyclone (AVFH) with an annular vortex finder (AVF) is commonplace in hydrocyclone commissioning in such applications. This study aims to uncover and investigate some of the issues that raise when it comes to configure and create a product promise for these devices via numerical methods. Two-phase, steady state, 3D AVFH models using the Standard k-ε turbulence model has been created and optimized in terms of particle residence times and separation efficiencies to conform with the published experimental data of a similar procedure. Simulations show that by adapting particle time-step parameter in a pseudo-transient discrete element modeling (DEM) setting, AVFH with different throughput properties can be confidently modeled and the results can be extrapolated to involve excessive operating conditions.

1 Introduction

Possible solutions for the cost-efficient and effective separation of immiscible fluid-fluid and fluid-solid mixtures are provided by the development of non-thermal separation techniques. One of the most prevalent non-thermal separation technologies features hydrocyclones, whose widespread application can be attributed to its compact design and low power requirements. Separation of immiscible fluids is crucial to reduce environmental pollution, improve the quality of product, and achieve maximum industrial process. Traditional separation technologies, such as distillation, centrifugation, and membrane filtration, have widely been used but are energy-intensive, costly, and inefficient in treating low-concentration or emulsified oil-water mixtures [1, 2]. For instance, distillation requires high amounts of thermal energy, while centrifugation is costly to purchase and maintain due to the presence of moving parts. These shortcomings have led to the invention of more efficient, cost-effective, and environmentally sustainable separation technologies [3].

* Corresponding author: orcun.ekin@adu.edu.tr

Hydrocyclones have been a good choice because they are compact, support high flow rates, and low energy consumption. Hydrocyclones function by employing centrifugal forces developed by the difference in phase density to separate liquids, making them ideal for non-thermal separation processes. Hydrocyclones are applied globally in petrochemical, energy, and food processing industries, where they carry out the separation of oil-water emulsions with no input of thermal energy and no complex mechanical equipment [4]. However, even with their optimal attributes, hydrocyclones are plagued by one significant disadvantage: short-circuit flow (SCF). SCF is an occurrence where unseparated fluid bypasses the separation process and exits through the top overflow pipe, reducing the overall separation efficiency. This impact is particularly unwanted in hydrocyclones used for dewatering, where water is meant to be drained from oil, as SCF will carry water droplets into the overflow and thus contaminate the oil phase [5].

In order to address the issue of SCF, researchers have suggested new geometries, some of which are the annular vortex finder hydrocyclone (AVFH). The AVFH possesses an annular vortex finder (AVF), which actively deflects SCF, preventing unseparated fluid from premature escape and significantly improving separation performance. Experimental studies, such as those conducted by Zhao et al. [5], have demonstrated the effectiveness of the AVFH in reducing SCF and enhancing separation efficiency. In their study, the AVFH-S (a specific type of the aforementioned AVFH) indicated a maximum separation efficiency of 84.71% that was 4.90% greater than that which is achieved using a conventional hydrocyclone. Further, the AVFH-S reduced the SCF rate to 0% at an inlet speed of 5 m/s, proving that it can significantly remove the issue of SCF.

Though experimental results provide crucial insight into AVFH performance, a deeper exploration of the flow dynamics and opportunities for optimization requires a more advanced approach. Computational Fluid Dynamics (CFD) offers a sound method of scrutinizing the complex flow fields of hydrocyclones, enabling the researcher to analyze the influence of key parameters such as AVF insertion depth, inlet velocity, and multiphase flow behavior. For instance, studies like Liu et al. [6] and Zhao et al. [7] have utilized CFD to investigate the flow pattern and separation behavior in hydrocyclones and demonstrate the way in which efficiency can be enhanced by structure adjustment. However, a reliable, structured model to answer and adapt to the changes in system parameters such as throughput rates, counter-pressure readings, split-ratios etc. may prove difficult, even impossible in some numerical cases. Although successful simulation of these parameters can provide a holistic view of the underlying processes of greater efficiency in AVFH, in combination with experimental data and serve as a basis for further optimization.

This specific study addresses and attempts to solve the issues the author faced in the 3D modeling of AVF hydrocyclones in terms of CFD-DEM parameterization and implementation. Although the models suggested aim to numerically represent the flow field and separation behavior of the AVFH, the main novelty of the study stems from addressing the consistent issue of particle time-step (PTS) selection in discrete particle modeling for such systems. Although several previous works, for example the study of Zhao et al. [7] revealed the geometric alterations to hydrocyclone modeling, such as extending the AVF insertion which gradually lowers the SCF rate and raises the efficiency in separation, there is a significant gap in terms of testing and improving the device effectiveness via numerical methods. Therefore, in this study, by combining experimental data with CFD simulations, the author tries to identify the optimum design parameters for AVFH so that there is numerical efficiency over a wide range of operating conditions and more importantly, a basis to an adaptive, reliable mathematical model. Through simulation of the effect of critical parameters such as AVF insertion depth, inlet velocity, and multiphase flow properties, the study aims to uncover the mechanism of improved efficiency. The outcome of the numerical analysis not only verifies experimental results but also form a basis for minimizing future hydrocyclone design through making it more efficient for utilitarian application. The acquired knowledge from this study will drive efforts to reduce energy consumption and save the environment in oil-water separation, which ultimately will benefit industries worldwide.

2 Material and method

This study adopts the experimental dataset of an AVF hydrocyclone published elsewhere [5] to investigate some of the process-specific aspects and CFD modeling issues, as stated previously. The modeling methodology adopted to configure and solve the predefined issue will be explained elaborately in the following sections.

2.1 Problem definition

Although 3D modeling of an existing or conceptual flow device is a relatively straightforward task, testing the product-promise using finite element methods, many times due to the intricate physics involved, might become an obstacle for engineers. Determining proper particle time-steps for discrete element modeling (DEM) is one of those hurdles. The reason is that, even when the same settings, such as mesh structure or some of the boundary conditions (BC), are utilized over and over, changing inlet conditions for flow devices usually require alternating particle time-steps in particle-laden flows. The study aims to address this issue by picking the best possible particle time-step parameter for each inlet BC. The geometric details of the model can be seen on Figure 1.

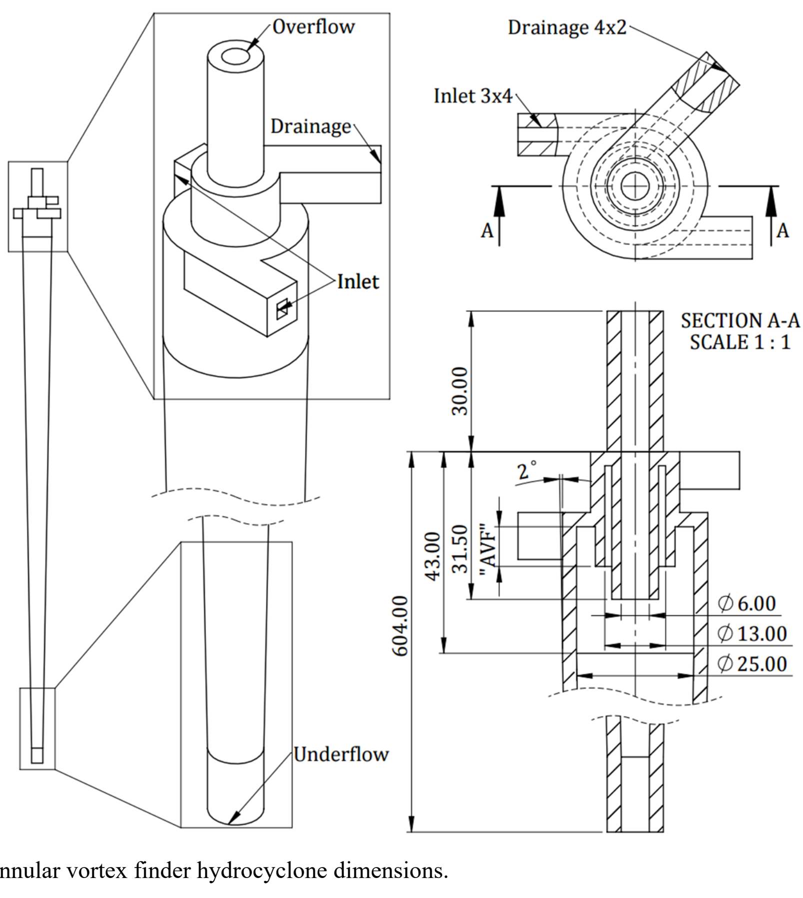

Fig. 1. Annular vortex finder hydrocyclone dimensions.

This study uses a Eulerian-Lagrangian approach as water droplets to be separated are considered as discrete phase, hence the Lagrangian approach [8]. Water droplets within the white oil behaving as solid particles is the main assumption this study suggests which affects every result displayed in the following titles. Water droplets have the same physical properties at every location of the hydrocyclone and do not interact with one another, that is, no contact models and no merge or split dynamics were introduced.

In solving particle laden momentum and mass conservation equations, Reynolds averaged Navier-Stokes (RANS) methods, more specifically the two-equation Standard k-ε model was utilized. As an addition, another popular RANS method for hydrocyclone modeling, Reynolds Stress Model [9-11] was tested against the same operating and boundary conditions, however due to the reasons stated in this study, Standard k-ε model proves to be the more efficient and reliable choice between the two. Following titles describe the mathematical mainframe for continuous and discrete phases in terms of the Standard k-ε model.

2.2 Continuous phase

The turbulent viscosity μ_T can be calculated using Eqn. (1):

$$\mu_T = \rho C_\mu \frac{k^2}{\varepsilon} \tag{1}$$

whereas the transport equation of turbulent kinetic energy k is as follows:

$$\rho(u \cdot \nabla)k = \nabla \cdot \left[\left(\mu + \frac{\mu_T}{\sigma_k}\right)\nabla k\right] + P_k - \rho\varepsilon \tag{2}$$

and the transport equation of turbulent dissipation rate ε is:

$$\rho(u \cdot \nabla)\varepsilon = \nabla \cdot \left[\left(\mu + \frac{\mu_T}{\sigma_\varepsilon}\right)\nabla \varepsilon\right] + C_{\varepsilon 1}\frac{\varepsilon}{k}P_k - C_{\varepsilon 2}\frac{\varepsilon^2}{k}, \varepsilon = ep \tag{3}$$

with the production term, P_k defined as [12]:

$$P_k = \mu_T[\nabla u \colon \left(\nabla u + (\nabla u)^T - \frac{2}{3}(\nabla \cdot u)^2\right] - \frac{2}{3}\rho k \nabla \cdot u \tag{4}$$

The empirical constants associated with Standard k-ε model are defined as follows: $C_\mu = 0.09$, $C_{\varepsilon 1} = 1.44$, $C_{\varepsilon 2} = 1.92$, $\sigma_\varepsilon = 1.3$ and $\sigma_k = 1.0$ as stated in [13].

2.3 Discrete phase flow

The term phase in discrete element modeling refers to the particles within the continuous medium and not a ‘phase’ of the continuous liquid, i.e. gas phase or solid phase. Within that context, the governing equations for the particle motion are shown in Eqn.’s (5)-(8):

$$m_p \frac{d\vec{u}_p}{dt} = m_p\vec{g} - \rho\vec{g}V_p + \vec{F}_D + \vec{F}_a \tag{5}$$

where m_p is the particle mass; $\vec{u}_p$ is the particle velocity; t is the time; $\vec{g}$ is the gravitational acceleration; ρ is the oil density; V_p is the particle volume; and $\vec{F}_D + \vec{F}_a$ is the fluid-particle interaction force term with $\vec{F}_D$ is the drag force and $\vec{F}_a$ is additional force. Here, the drag force $\vec{F}_D$ is evaluated by Eqn. (7):

$$F_D = \frac{18\mu}{\rho_p d_p^2}\frac{C_D Re}{24}(\vec{u} - \vec{u}_p) \tag{6}$$

Here, u and u_p represent the velocities of the continuous medium and the particle, respectively, ρ_p is the densities of the medium and the particle, and d_p is the particle diameter, C_D is the drag coefficient; $\vec{u}$ is the fluid velocity; and Re is the relative Reynolds number calculated by Eqn. (8).

$$Re = \frac{\rho d_p}{\mu}\left|\vec{u}_p - \vec{u}\right| \tag{7}$$

Besides, to obtain accurate results, the “virtual mass” force, Saffman’s lift force and pressure gradient force were used as additional forces to simulate the particle motion, as seen on Eqn. (8):

$$\vec{F}_a = C_{vm}\frac{\rho}{\rho_p}\left(\vec{u}_p\nabla\vec{u} - \frac{d\vec{u}_p}{dt}\right) + \frac{\rho}{\rho_p}\vec{u}_p\nabla\vec{u} + \frac{2K_{sl}\sqrt{v}\rho d_{ij}}{\rho_p d_p (d_{lk}d_{kl})^{\frac{1}{4}}}(\vec{u} - \vec{u}_p) \tag{8}$$

where C_{vm} is the virtual mass factor with a value of 0.5; $K_{sl} = 2.594$; d_{ij} is the deformation tensor; the first group of terms on the right-hand side of the equation is called the virtual mass force, while second group is Saffman’s lift force and third group is pressure gradient force. With that, the DEM mainframe suggested in this study entails several assumptions to the discrete phase: water droplets were considered to be rigid particles of uniform size. Also, the particle-particle interactions that would otherwise be a critical aspect of model equations were ignored. These assumptions were made to build and validate a lean numerical model to conform with the experimental study considered in [11] and on the basis of the disperse nature of water droplets within white oil.

2.4 Meshing and numerical strategy

A hexa-dominant meshing strategy was adopted due to the cylindrical nature of the model. Cylindrical geometries usually allow sweep meshing, therefore a fully hexahedral mesh structure. The current model however involves some features (the inlet and drainage lines into and out of the hydrocyclone) that made a fully-swept mesh impossible. However, the current mesh utilizes hexahedral elements as a majority finite element type. Some of the sharp edges and angles as well as joining surfaces of inlet and outlets were meshed using four-faceted wedge elements, as seen on Figure 2.

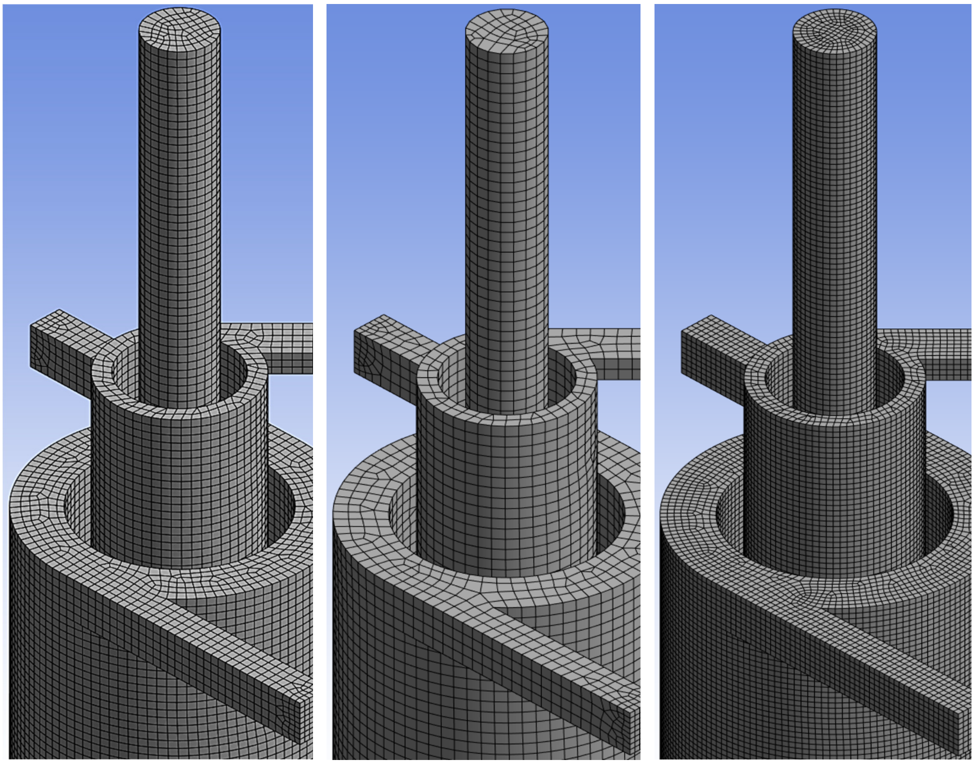

a) b) c)

Fig. 2. Mesh sensitivity visuals on three variations: (a) optimum; Mesh#2, (b) coarse; Mesh #1 and (c) fine; Mesh#3.

A mesh sensitivity analysis to verify an appropriate mesh structure with minimum number of elements was performed considering split ratio value for 5 m/s inlet condition (as the average inlet velocity or throughput rate). The results show that Mesh#2 was the optimum choice for the current study, with a relative change between the finer mesh option in Mesh#3 of 1.08%. Since the difference obtained was negligible compared to the difference between Mesh#2 and Mesh#1 (the 'coarse' mesh), Mesh#2 was selected. Details of all configurations can be seen on Table 1.

Table 1. Mesh sensitivity study.

Mesh Reference	Element Min. Size	Avg. Ortho Quality	# of Elements	Hydrocyclone Split Ratio (CFD)	Difference
Mesh #1	0.5mm	0.72645	308399	55.00%	-
Mesh #2	0.75mm	0.74868	685181	58.46%	5.92%
Mesh #3	1mm	0.78836	2038119	59.10%	1.08%

The AVFH hydrocyclone operates on white-oil (with $821.57\ kg/m^3$ density and $0.01056\ Pa \cdot s$ dynamic viscosity) with a 0.5% water ($980\ kg/m^3$ density) content. As stated previously, water droplets act as a discrete phase, with constant diameter ($13.5 \mu m$).

Therefore, only the density of water was coined into the simulations and not the viscosity. All outlets from the hydrocyclone are at zero-gauge pressure (i.e., atmospheric pressure), that is, no counter-pressure was applied, as per the source material. No heat transfer equation was involved; therefore, the simulations represent isothermal conditions. Model specific boundary conditions for both continuous flow and discrete phase are summarized in Table 2.

Table 2. Model BC table for continuous medium and discrete phase.

Boundary Name	Continuous Phase	Value (Cont. Phase)	Discrete Phase
Inlet	Velocity Inlet	Variable (3-7m/s)	Particle Injection (Zero relative velocity)
Overflow	Pressure Outlet	Gauge Pressure (0 atm)	Particles Escape
Drainage	Pressure Outlet	Gauge Pressure (0 atm)	Particles Escape
Underflow	Pressure Outlet	Gauge Pressure (0 atm)	Particles Trapped
Walls	Stationary, No-slip	Reflect (Elastic Collision)	-

The numerical scheme was structured considering two main RANS modeling approaches; the Standard k-ε Model and Reynolds Stress Model (RSM), the latter being suggested to reflect recent studies involving numerical modeling of hydrocyclones. Referring to Zhang et al.'s study [10], Reynolds Stress Model (RSM) has been confirmed to simulate the anisotropic turbulence with better efficiency, which is considered to be a characteristic of hydrocyclones [9-11]. However, in this study, the Standard k-ε model produced better residual error figures over the solver iterations in terms of critical parameters, was considerably faster in comparison, and validated the experimental results just as competitively as RSM (please refer to the model validation next page). Therefore, the author ultimately decided to work with the Standard k-ε model, potentially in spite of some contemporary work, to display the particle time-step aspect of CFD-DEM in hydrocyclone analysis.

3 Results and discussion

The validation was performed in terms of comparing the dewatering success of the numerical model to the experimental setup, adopted from the [5]. As seen clearly on Figure 3 and to emphasize again the prospect of this study, once the particle time-steps are established, the numerical data -almost perfectly follows the experimental results for both RANS models. The author is confident to state that under certain conditions, the model suggested in this study can be considered as validated. However, the particle time-step relation will be discussed further in the following displays of model performance.

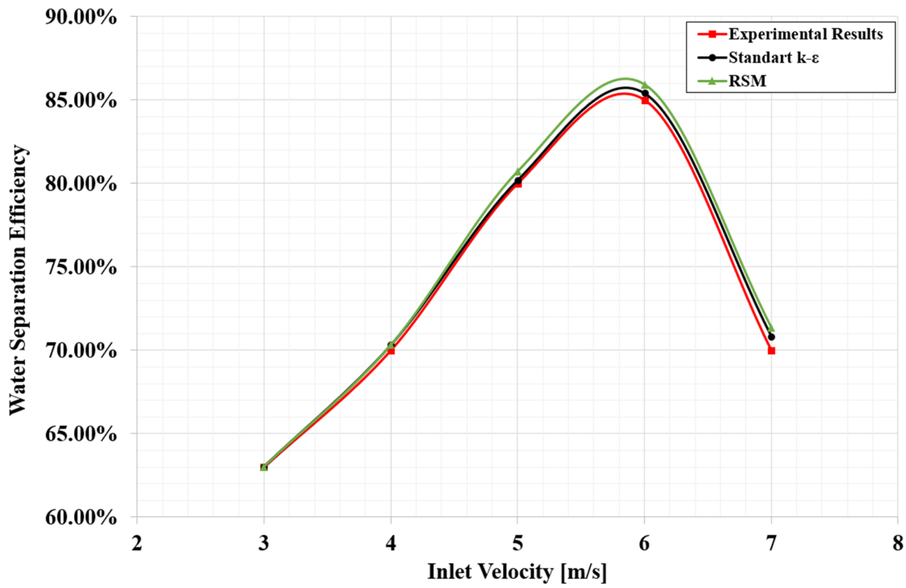

Fig. 3. Validation of both RANS models against experimental results published elsewhere.

Point-for-point error analysis presented in Table 3 also shows a close follow-up from the both models, the Standard k-ε and RSM. However, the fact that this was due to setting particle time-steps precisely to conform the experimental results requires further assessment as to which RANS model performs better. This display also emphasizes the particle time-step playing a key role in model validation which can be 'adjusted'. Residual errors, on the other hand prove the Standard k-ε model is the more appropriate choice in the context of AVF hydrocyclones.

Table 3. Separation efficiency validation details for both models.

Inlet Velocity [m/s]	Separation Efficiency (Experimental)	Separation Efficiency (Standard k-ε)	Standard k-ε Relative Error	Separation Efficiency (RSM)	RSM Relative Error
3	63.00%	63.02%	0.03%	63.02%	0.03%
4	70.00%	70.31%	0.44%	70.31%	0.44%
5	80.00%	80.21%	0.26%	80.73%	0.90%
6	85.00%	85.42%	0.49%	85.94%	1.09%
7	70.00%	70.83%	1.18%	71.35%	1.90%

Figure 4 shows the residual monitors after 500 iterations for both models (ANSYS Workbench 2025R2, 'Student Version'). Of the Standard k-ε and RSM results on 5 m/s inlet velocity (as the average value), the latter displays a non-convergent behavior, despite the fact that simulation results still conforming the experiments. Although continuity residual on the Standard k-ε is stabilized around 1.4×10^{-3}, all other parameters drop well below 1×10^{-6} order, proving the Standard k-ε performs better in all-default settings. Objectively, both RANS models were run with all-default settings. However, this was to be expected, as this study was not established to be a multi-parameter analysis of the phenomenon, but a particle time-step investigation.

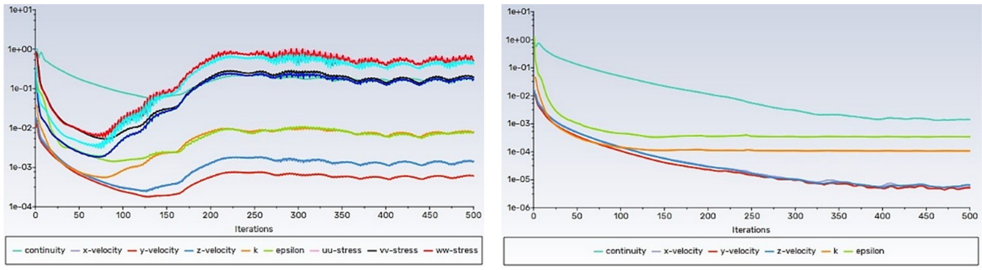

a) b)

Fig. 4. Side-by-side comparison of RSM (a) and the Standard k-ε methods after the first 500 iterations (b).

Streamlines for the 3 m/s and 7 m/s inlet velocities show swirl sections near the inlet region but otherwise a laminar flow regime leaving the hydrocyclone through overflow and drainage outlets, as seen on Figure 5. Even in those regions where a swirling flow can be observed, no vorticity was detected, as will be seen on the Figure 6 as well, where anisotropic turbulence was of no great concern. This is to further solidify that as long as residual behavior of critical simulation parameters are acceptable and model results validate the respective experimental data, the Standard k-ε RANS model is as good as RSM in the context of hydrocyclone modeling. Although the reader might see further comparison of these two models in the following pages, they are mostly confined to diagrams. The contour graphs will contain data generated via the Standard k-ε model results.

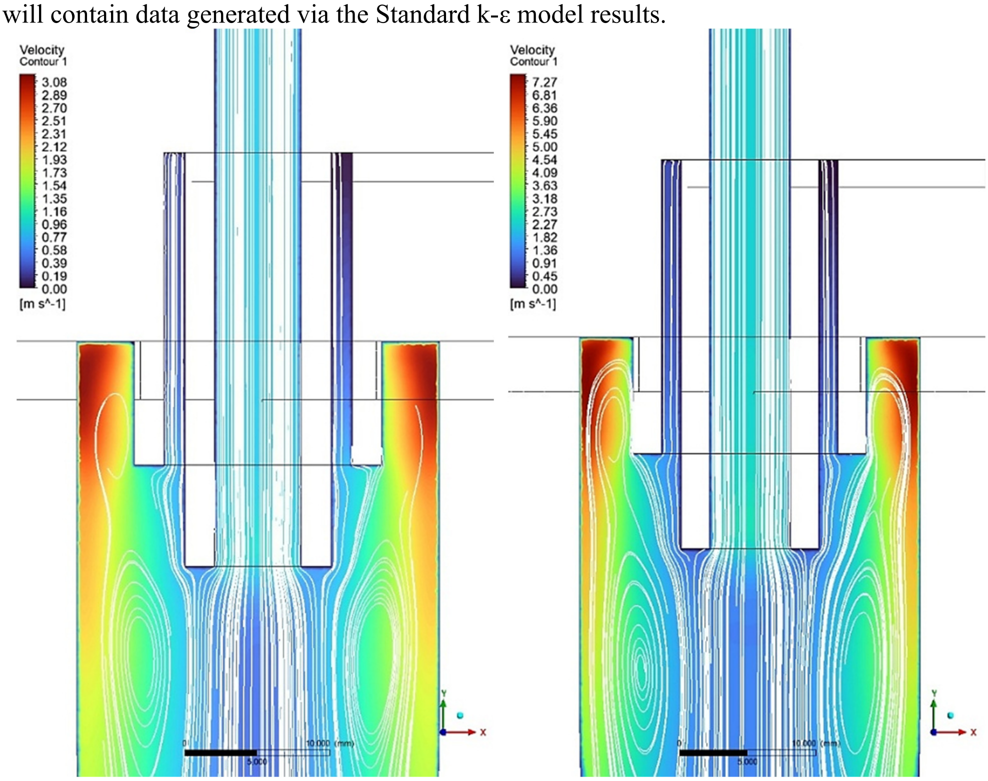

a) b)

Fig. 5. Velocity streamlines for 3m/s (a) and 7ms inlet velocities (b).

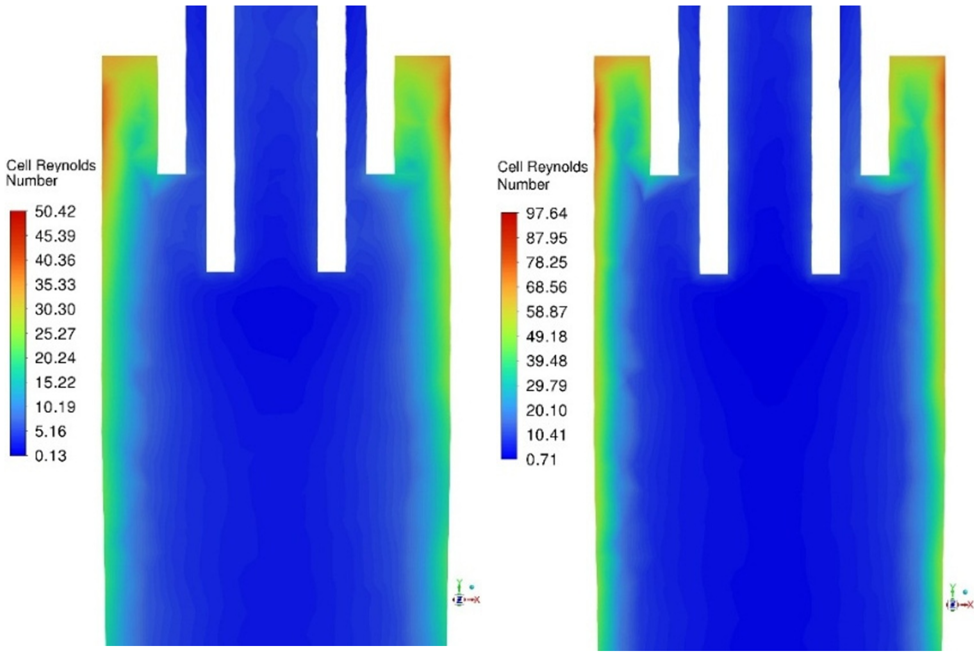

a) b)

Fig. 6. Local Re number distribution along the center plane of AVF hydrocyclone for (a) 3m/s and (b) 7m/s inlet velocities.

Figure 7 reports 2D and 3D vector graphs to characterize the continuous fluid behavior in the vicinity of the most 'chaotic' region of the AVF hydrocyclone: the inlet, drainage and overflow channels converge in the cylindrical upper-section of the geometry. The two figures on top display the flow regime for 3 m/s inlet velocity, whereas the bottom two figures represent 7 m/s inlet boundary condition. One striking detail is that, in accordance with the streamline graphs on Figure 5, both 2D and 3D graphs show a laminar discharge on both outlets: overflow and drainage. As a reminder, the outlet named 'drainage' is actually the continuation of the AVF in this geometry and the stream of flow captured through it is called 'short circuit', which is the purpose of an AVF geometry in hydrocyclones [5].

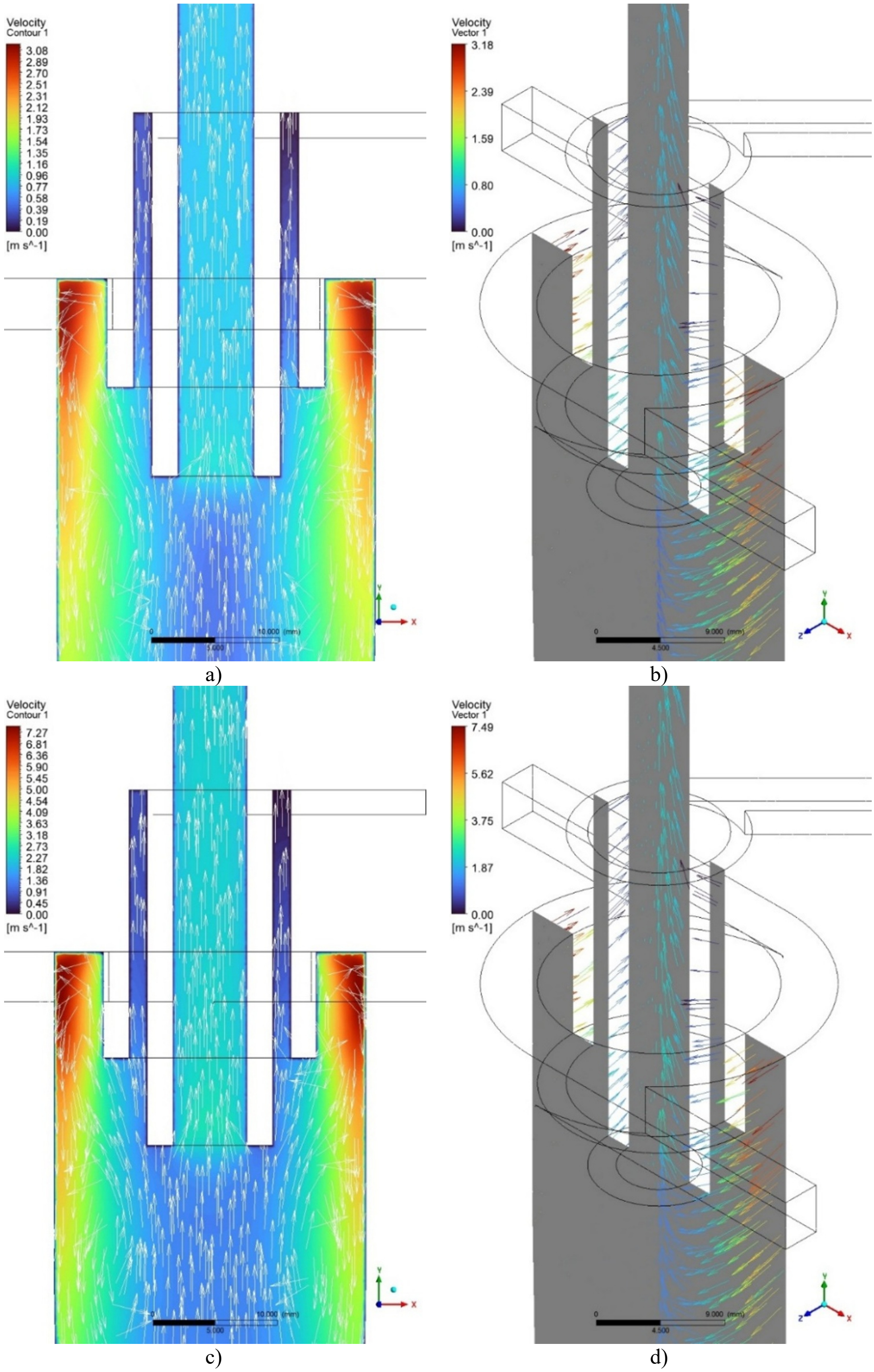

Fig. 7. 2D and 3D vector graph presentations of 3 m/s (on (a) and (b)) and 7 m/s (on (c) and (d)) inlet velocities.

As suggested previously, the main prospect of the current study was to investigate the particle time-step parameter effect on the separation efficiency. Extensive research was done towards understanding this relation, a very brief summary of which can be seen of Figure 8. As the reader will remember from the validation data set discussed in Figure 3, particle time-step adjusted Standard k-ε and RSM algorithms provide very close representation of experimental separation efficiency for the AVF hydrocyclone. This tendency was lost however, as soon as a single particle time-step to represent all inlet BCs was used. As can be seen on Figure 8, the Standard k-ε model promptly fail when max. or min. time-step value is utilized as the common parameter. Similarly, RSM model also fails when the separate time-steps optimized for the Standard k-ε model is used as RSM particle time-steps. As this was the common issue with both RANS models, no max. or min. time-steps were applied in the RSM case.

Following the RANS performance, an extrapolation for the particle time-steps for the possible inlet velocities exceeding 7 m/s was suggested. These results can be seen on Figure 9 [5]. In generating the trendlines, adapted time-steps for both RANS models were utilized. The results indicate that as inlet velocities -or hydrocyclone throughput rates in this context- increase, smaller and smaller particle time-steps are required to keep the CFD-DEM approach valid.

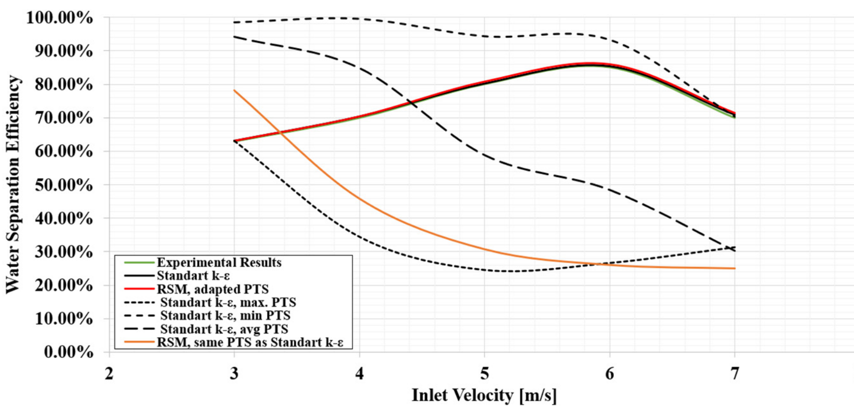

Fig. 8. Separation efficiency for all variations considered.

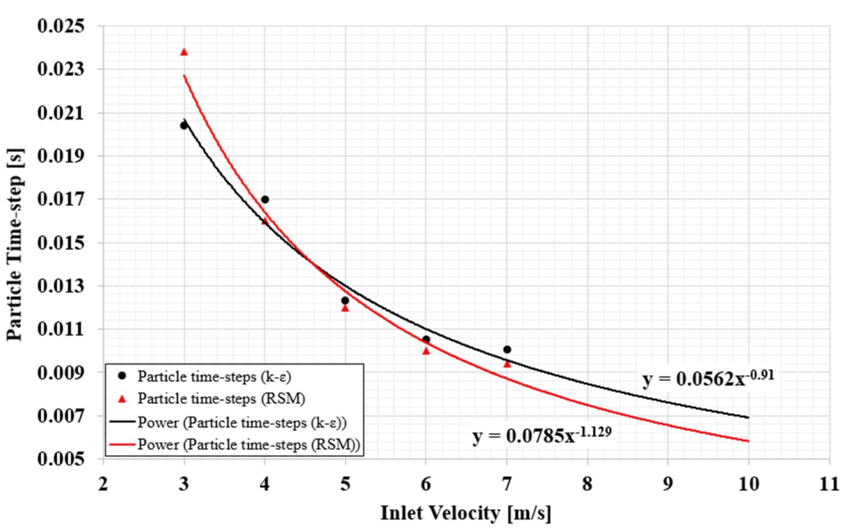

Fig. 9. Extrapolation for PT estimations beyond the experimental values.

Another important factor when it comes to hydrocyclones is the split ratio, that is the ratio of 'underflow' mass flow to that of hydrocyclone inlet mass flow. Again, when both turbulence modeling algorithms are considered, the tendency is that the split ratio drops as inlet mass flow (in the diagram, the inlet velocity) is increased. The details can be seen on Figure 10. However, the author would like to emphasize the offset between the two RANS models: the Standard k-ε shows an almost negligible drop going from min. to max. throughput rate, whereas RSM suggests a drop in the vicinity of 2.5%. As there is no suggestion of split ratio change of drastic proportions in the referenced article [14], further research is required in this particular area. The reader should also note that although in the current context the Standard k-ε is preferred and validated, RSM would be the more convenient choice of RANS method as it becomes prominent in the presence of anisotropic turbulence, a characteristic of hydrocyclone flows [11].

The parameters investigated in this study also include particle residence times for different inlet conditions. Particle residence time (PRT) is defined as the duration particles remain within a specific system, in this case, hydrocyclone volume. As ANSYS Fluent does not generate a solver parameter for the PRT and it cannot be extracted from the particle track files (possible perhaps using a user-defined function but not directly), the author presents particle tracking visuals to characterize the PRT for different inlet velocities.

Figure 11 demonstrates that a fraction of water droplets is extracted immediately through the overflow-drainage lines, hence the blue ('colder' tones indicate shorter PRTs) coloration of individual particle tracks near that region. This scheme changes however, as droplets -due to density difference start propagating downward, through the underflow area (the long, conical section of hydrocyclone). These tracks gradually shift to color red (warmer tones indicating longer PRTs), and extracted from the separation volume as 'separated'. In terms of particle fates, droplets extracted either from underflow or drainage lines are counted as separated, hence increasing the separation efficiency. It is important to note that PTS parameter inevitably affects PRTs of particles, in the form of precision tracking of particle momenta and positions. Arguably, the PRT figures along with particle trajectories might be better calculated with ever decreasing PTS values; smaller the time-step, shorter the distance traversed by a particle, hence less the residual error. However, as the above results of the study show, there should be an agreement between PTS and experimental separation efficiency of hydrocyclone to validate a CFD-DEM model as well, which in turn brings a structure in PRT monitoring.

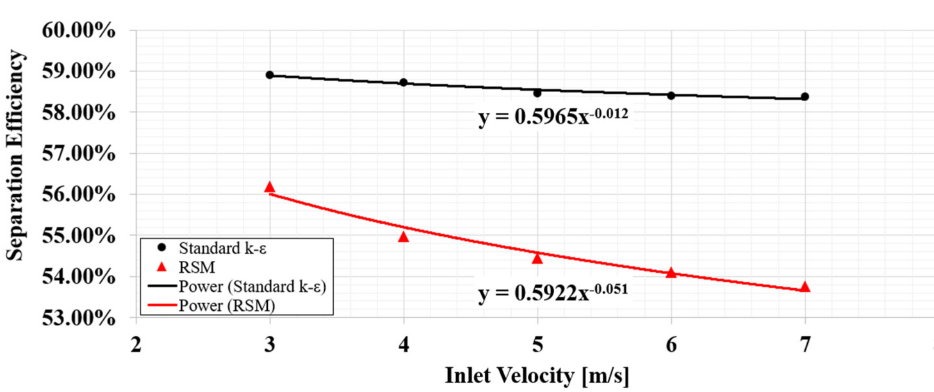

Fig. 10. Hydrocyclone Split Ratios for both RANS model results.

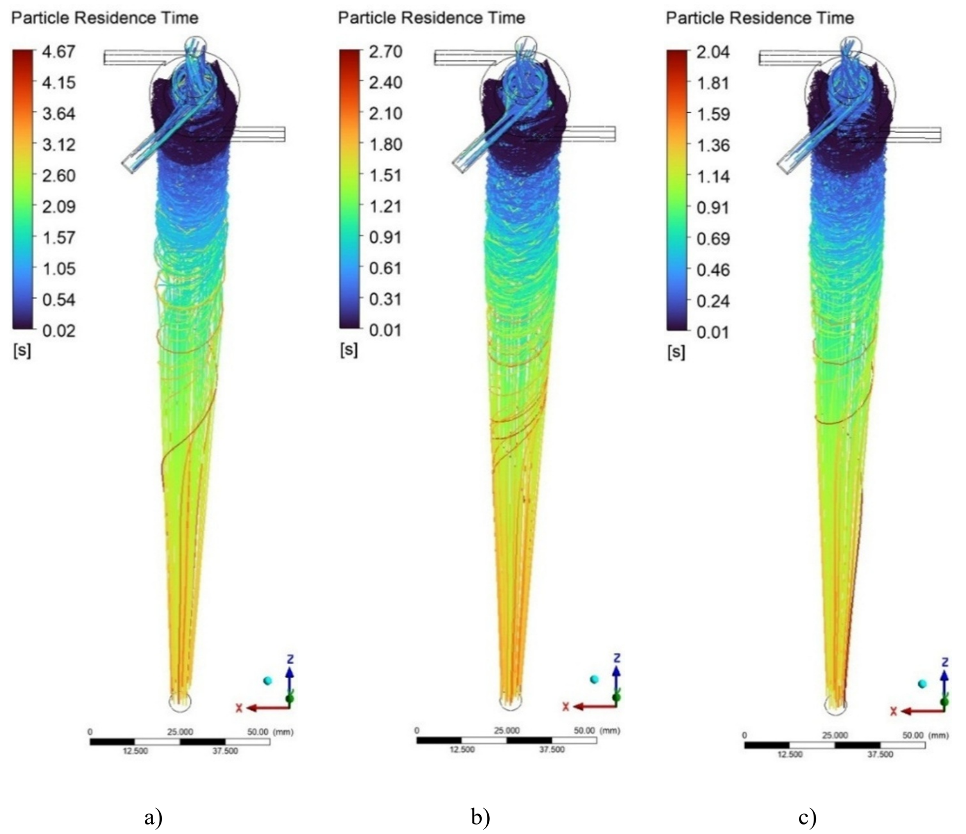

Fig. 11. Particle residence time comparison for the Standard k-ε model for (a) 3 m/s, (b) 5 m/s and (c) 7 m/s inlet velocity BC.

4 Conclusion

A finite element model -or approximate model requires validity over a certain interval of parameters to be practical. When there are multiple physics involving, such as immiscible phases of liquids or particles in a fluid matrix, finding the appropriate settings to render this model practical may become a challenge. The current settings and approach provided hydrocyclone models that can operate at agreeable margins of error, reaching around 2% at maximum (see Table 3). Having verified against experimental studies, the simulations revealed a mostly laminar flow regime through the underflow region of the hydrocyclone, with linear velocities reaching up to 7.27m/s, depending on the inlet velocity. Another implication of the simulations suggests that with increasing inlet flow rate, the PTS should be reduced accordingly to maintain model success: 10m/s inlet velocity requires 0.007s PTS according to the inference seen on Figure 9. The implications of these findings state that through CFD-DEM modelling with precision tuning towards PTS parameter, the properties such as hydrocyclone flow regime, SCF and particle trajectories can be easily visualized. A validated model provides the researcher with information concerning PRT values for the discrete phase and hydrocyclone split ratios that otherwise would require extensive measurement work. With that note, the study, as the reader would certainly notice, leaves some important follow-up points:

As mentioned above, the discrete element background involves several assumptions such as water droplets being assumed rigids particles of uniform size and no particle-particle interactions. However, in reality, the droplets may very well interact, which suggests not only elasticity to the discrete phase, but also a variable number of elements and cluster sizes along the simulations. These properties were ignored after exponentially increasing computational demand and overall model complexity were observed.

Along with hexahedral mesh structure, tetragonal or polyhedral meshes could be tested against the same parameters to see the pros and cons of the respective methods.

Experimental data and CFD-DEM comparisons over hydrocyclone split ratios could be developed and the results could be extended to cover the annular vortex finder variants, such as long and wide VF geometries, at different inlet conditions.

Another possible improvement could be made by adjusting the turbulence model constants, instead of the PRT parameter. In the author's defence, adjusting the turbulence model parameters is not for the layman who uses engineering software just to test a product-promise or fast modeling to test other process parameters.

References

1. J. He, J. Yang, G. Xu, X. Fu, X. Hao. The investigation on the ceiling of inlet velocity regarding to fine particle separation in a cyclone. Powder Technol., **444**, 120028 (2024). https://doi.org/10.1016/j.powtec.2024.120028
2. J.B. Starrett, K.P. Galvin. Application of inclined channels in the hydrodynamic classification of minerals by particle size – extension to coarser separations. Miner. Eng., **222**, 109114 (2025). https://doi.org/10.1016/j.mineng.2024.109114
3. W.I. Mazyana, A. Ahmadi, J. Brinkerhoff, H. Ahmed, M. Hoorfar. Enhancement of cyclone solid particle separation performance based on geometrical modification: Numerical analysis. Sep. Purif. Technol., **191**, 276285 (2018). https://doi.org/10.1016/j.seppur.2017.09.040
4. S. Zhang, J. Jing, M. Luo, M. Qin, F. Zhang, L. Yuan. Experimental study on hydrocyclone desanding of high-viscosity oil. Fuel, **341**, 127691 (2023). https://doi.org/10.1016/j.fuel.2023.127691
5. W. Zhao, J. Li, T. Zhang, A. Wei, S. Li, D. Yang, X. Yang, X. Jiang, H. Wang. Separation characters of dewatering hydrocyclone with annular vortex finder based on particle image velocimetry and experiments. Sep. Purif. Technol., **353**, 128619 (2025). https://doi.org/10.1016/j.seppur.2024.128619
6. P. Liu, D. Hou, Q. Zhao, L. Jiang, B. Cui, D. Wei, W. Yin. Research on the separation chamber diameter ratio of the multi-stage hydrocyclone to inhibit particle misplacement. Adv. Powder Technol., **35**, 104418 (2024). https://doi.org/10.1016/j.apt.2024.104418
7. Q. Zhao, B. Cui, A. Ji, T. Song, Y. Shen. Experimental and numerical study of the effect of particle size distribution on hydrocyclone classification. Adv. Powder Technol., **35**, 104398 (2024). https://doi.org/10.1016/j.apt.2024.104398
8. O. Ekin. A Numerical Analysis on the Submicron- and Micron-sized Particle Sedimentation in a Wire-to-plate Electrostatic Precipitator. KSU Journal of Engineering Sciences (KSU JES), **27**, 7891 (2024). https://doi.org/10.17780/ksujes.1354863
9. J. Tian, L. Ni, T. Song, Z. Jianing. CFD simulation of hydrocyclone-separation performance influenced by reflux device and different vortex-finder lengths. Sep. Purif. Technol., **233**, 116013 (2020). https://doi.org/10.1016/j.seppur.2019.116013

10. Y. Zhang, M. Xu, W. Hu, X. Xu, Q. Zhang. Vortex finder diameter and depth effects on the separation performance of hydrocyclone. Chem. Eng. Res. Des., **195**, 181191 (2025). https://doi.org/10.1016/j.cherd.2023.05.052
11. Z. W. Zhang, Q. Li, Y. H. Zhang, H. L. Wang. Simulation and experimental study of effect of vortex finder structural parameters on cyclone separator performance. Sep. Purif. Technol., **286**, 120394 (2022). https://doi.org/10.1016/j.seppur.2021.120394
12. L. Davidson. An Introduction to Turbulence Models (Chalmers University of Technology, Göteborg, Sweden, 2022)
13. M. Gong, X. Zhang, Y. Shen, W. Huang. Numerical analysis of engine idle wake thermal field based on Standard k-ε model and optimization of safety zone. Therm. Sci. Eng. Prog., **69**, 104432 (2026). https://doi.org/10.1016/j.tsep.2025.104432
14. V. T. Hashe, T. J. Kunene. Numerical Analysis of the Effect of the Vortex Finder on the Hydrocyclone's Split Water Ratio and Separation Performance. Math. Comput. Appl., **28**, 50 (2023). https://doi.org/10.3[390/mca28020050